# On characterizing and simulating porous media
# W. L. Gore and Associates

Report prepared by: P. Sanaei, V. Ciocanel,

Other problem participants: S. Bohun, C. Breward, P. Dubovski,

D. Schwendeman, H. Yaple, S. Ahmed, J. Batista, M. Hennessey,

T. Hueckel, S. Iyaniwura, F. Meng, M. Mohebujjaman,

Y. Qian, D. Serino, O. Shonibare, S. Hill, B. Tille, D. Rumschitzki,

C. Bi, J. Sexton, Y. Chen, J. Duan, T. Gu, Q. Wang, D. Duffy, M. Zyskin

January 15, 2017

## 1   Introduction

For MPI 2016, Gore brought three distinct problems to the workshop and the participants broke up into three separate groups, each group focussing on a separate problems. The problems were:

1. Develop a mathematical model describing the production and flow of fluid in a sulfur dioxide filter

2. Characterize the changes in properties of filters due to compression and other external forces

3. Develop and parallelize code for simulation of models for cellular growth on lattices

**Problem 1**

The first problem concerned the operation of a sulfur dioxide filter. In particular, to model the production and transportation of the fluid within the filter.

The efforts of the group were directed at developing a multi-scale model predicting the production of sulfuric acid on the scale of the entire filter by describing the generation of acid at the individual catalyst level, and homogenizing this local acid production to a continuum scale using an assumed porosity and packing of these catalysts.

Much of the initial investigation was invested in developing a model to predict the production of sulfuric acid at a single activated carbon pellet surrounded by sulfur dioxide. Given the conditions of 100% humidity and an abundance of oxygen, we only considered the change in concentration of the sulfur dioxide as it diffused through the acid layer and how the reaction at the catalyst surface affected the production of sulfuric acid. After generating and studying this model, attention was focused on the entire filter, modeling it as a continuous distribution of these individual pellets. From the pellet analysis, it was determined that the diffusion of gas through the filter was much faster than the generation of acid, and that at some maximal layer thickness (calculated using porosity at each portion of the filter as a measure of the average distance between pellets) the pores would be effectively sealed by the acid, blocking further diffusion of the sulfur dioxide from the channel. The resulting diffusion-advection model for the distribution of concentration of the sulfur dioxide in the filter and resulting generation of the acid was then used to predict the efficiency of the filter. A framework was developed that lends itself to including further refinements in the chemistry and the capability of simulating a variety of changes in the overall design of the filter.

**Problem 2**

The second group has concentrated on two problems. The first considers a filter comprised of randomly oriented fibers whose function is to filter out solute from a fluid that is forced through it. Apparently it is easy to carry out transport and filtration experiments on the filter material before it is rolled and inserted into canister, the form in which it is used by its customers. The process of insertion into the canister apparently compresses the filter material on the order of a factor of two, although the exact compression is not yet known, and the macroscopic flow and filtration properties become significantly different from the virgin filter material. The question that concerns Gore Inc.., the goal of this project, is to develop theory that allows the prediction of the transport properties of the packaged filter from the measured values of the same parameters on the virgin material.

We model the system by solving the filtration flow problem through a fiber matrix porous medium that is coupled to an advective-diffusion problem with an equation for the adsorption of tracer to the filter fibers. The coupling occurs due to 1. the filtration flow velocity field drives the solute advection; 2. the concentration profile in the filter drives solute adsorption to filter fibers, which modifies the void space distribution in the filter; 3. the local values of the transport parameters depend upon the local void space, fiber radius and fiber spacing; 4. the transport parameters, e.g., Darcy permeability, determine the pressure and velocity distribution. As such, one needs to set up and solve all parts of the problem simultaneously. Using physical parameter values from Gore, we have solved a one-dimensional version of the filtration and

advection-diffusion problem for the concentration of solute as a function of position throughout the filter for different times after initial filter use assuming an initial condition of a clean filter. We assume that the input pressure and concentration are given and time-independent. We then assume various compressions of the fiber matrix, which affect the transport parameters, and recalculate the tracer concentration vs position as a function of time. At the present moment the calculation does not include solute adsorption to filter fibers, and thus cannot yet account for filter clogging.

Future work will include accounting for solute adsorption to filter fibers and the resulting time-dependent reduction of filter efficiency and clogging. In addition, we shall allow for the alternative filter inlet boundary condition of prescribed fluid flow rate rather than pressure, which is more likely to represent the true industrial situation. Subproblem two of this section considers a model that relates the forces applied to the filter material during its insertion into its casing to the extent of filter deformation.

## Problem 3

The third group was developing a parallel framework to simulate the cell growth based on a 2D lattice considering the effect of the oxygen and nutrient concentration. This problem has been broken into five subtasks as follows.

First of all, we initialized the geometry of the biological system by specifying two types of objects - the lattice points on the dish and biological cells on the dish. For each lattice point element, we record the following fields - cell index, cell type, a list of neighboring lattice point elements corresponding to a different cell, as well as the concentrations of oxygen and nutrients. In terms of each biological cell object, we record the cell type in order to differentiate the four distinct types - the medium, the necrotic cells, the quiescent cells, and the proliferating ones. Additional fields are saved for the further simulations and for lattice updates, including a list of lattice spots composing the given cell and the average concentrations of oxygen and nutrients over the whole cell. These two types of objects will be linked through the cell indices. Then, we implemented the cell proliferation. In other words, given a cell object whose volume is the maximal volume allowed, this cell will be divided into two cells represented by two sets of connected lattice spots. This uniform cut has been carried out by treating the set of lattice spots as an undirected graph, and then using the breadth first search strategy to check the connectivity of its subgraphs. After considering the cellular function, our focus was placed on numerically solving the chemical reaction diffusion equations (as Partial Differential Equations) and parallelizing the solving procedure. We used ARKode, a numerical integration package with multiple types of parallelization. We built our simulation based on a 2D heat equation example, and implemented an appropriate reaction term and appropriate boundary conditions. As in
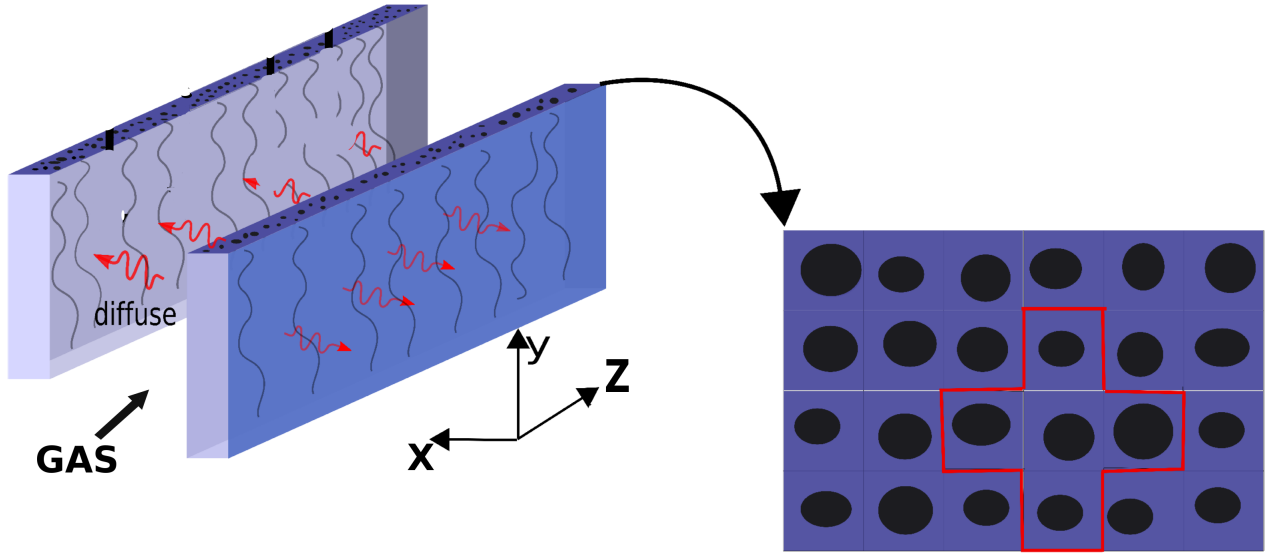
Figure 1: Direction of gas flow and diffusion, along and cross the panels respectively, and filter magnified cross section.

the example, we used a spatial domain decomposition. Moreover, we began implementing a parallel version of the Hamiltonian function which unitizes the domain decomposition to assign different lattice subdomain to available core processors. In the interior of each subdomain, the $H$ function is computed in a sequential fashion to avoid double counting. The computation on the boundary of each subdomain is handled by buffers which are carefully designed to communicate between different core processors. For the future work, we will integrate the above modules into a parallel framework for the simulation of the cell growth using Monte Carlo steps. We might also consider more complicated reaction and Hamiltonian function terms.

## 2    Modeling product transport in catalysts

Liquid production and transport within porous media is known to effect the performance of a wide range of technologies (fuel cells, venting, general catalysis, etc). In fuel cells, for example, water and acid are produced in a catalyst layer as a product of surface adsorption reactions. Once significant liquid is produced, it can push into the gas diffusion layer (GDL) and inhibit transport paths of reactants to the catalyst layer. A deeper understanding of fluid evolution within the porous media may help engineers to come up with more effective liquid management solutions. One of our goals in this workshop is to develop a mathematical model to predict and characterize fluid production/transport inside porous media. We are particularly interested in quantifying/predicting the time scale and spatial profile of flooding.
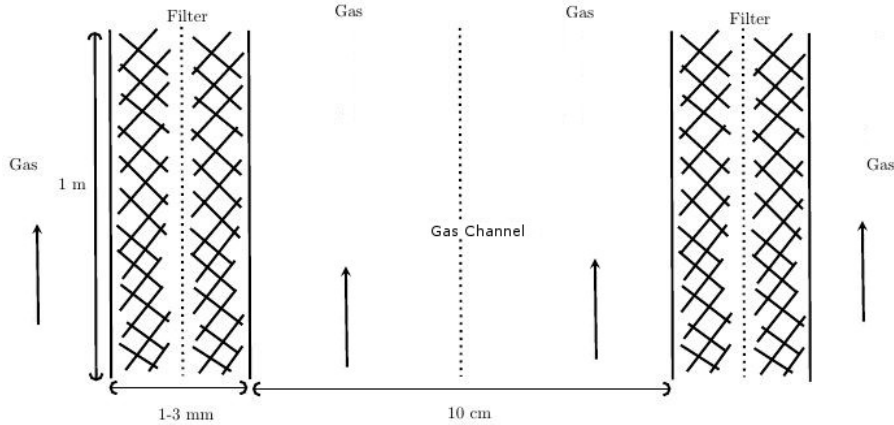
Figure 2: Macroscopic picture of the filter.

## 2.1 Modeling

The basic set up for the modeling in this section is as below. We have the gas flow which may contain some unpleasant gas such as Sulfur Dioxide, passes through the panels and parallel to them in $Z$-direction as shown in Figure 1. The panels to be modeled are long in $Y$-direction (about $l = 300 \; mm$) and the cross section of each of them has a thickness on the order of millimeters ($2H = 1 \; mm$) and a length in $Z$ direction on the order of meters (Figure 2). Because of symmetry, we just model half of the channel and filter and appropriate boundary condition were used, accordingly. The gas diffuses in to the panels along in $X$-axis, perpendicular to the gas flow direction and panels surface. There is no imposed flow or pressure jump in the inward direction across the filter. We suppose filters fibers to be arranged in a square repeating lattice stretch out along panels height. The diffused gas reacts with the filter fibers and the liquid is being produced in the porous media. It is assumed that the cross section of each filter consists of many catalyst which in fact make the reaction to be happened as

$$2SO_2 + O_2 + 2H_2O \rightarrow 2H_2SO_4. \tag{1}$$
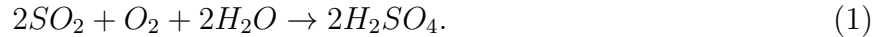
We use a coupled multi scale approach to tackle the problem: (i) small scale-analyze: the formation of sulfuric acid on the surface of a single filter pellet; (ii) large scale-analyze: the transport of sulfur dioxide in the gas channel and filter.

### 2.1.1 Small Scale–Analyze the formation of sulfuric acid on the surface of a single filter pellet

We consider spherical activated carbons (catalysts) with radius $R$, spread the whole filter and they react with the sulfur dioxide (gas) and the sulfuric acid (liquid) is formed, which occupies area around the catalysts. As shown in Figure 3, the liquid moves in the filter, while
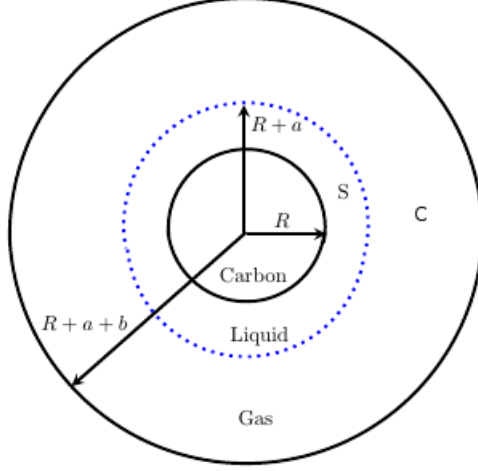
Figure 3: Schematic of activated carbon surrounded by sulfuric acid ($H_2SO_4$) and sulfur dioxide ($SO_2$).

concentration of sulfur dioxide decrease. We consider $a$ and $b$ as thickness of liquid (sulfuric acid) and gas (sulfur dioxide); respectively. Concentration of $O_2$ in the gas and liquid layers are $C_1$ and $C_2$; respectively, while $S_1$ and $S_2$ are concentration of sulfur dioxide in the mentioned layers. Here we ignore advection of $O_2$ and $SO_2$ in favor of diffusion, therefore the diffusion equation in the gas layer follows as

$$\frac{\partial C_1}{\partial t} = D_1 \nabla^2 C_1, \quad \frac{\partial S_1}{\partial t} = d_1 \nabla^2 S_1, \tag{2}$$

where $D_1$ and $d_1$ are diffusion coefficient of $O_2$ and $SO_2$; respectively with the far field boundary condition

$$C_1 \to C^*, \quad S_1 \to S^*, \quad \text{as} \quad r \to \infty. \tag{3}$$

We also have similar diffusion equations in the liquid layer for both $O_2$ and $SO_2$ with $D_2$ and $d_2$ as the correspondence diffusion coefficient in this layer.

$$\frac{\partial C_2}{\partial t} = D_2 \nabla^2 C_2, \quad \frac{\partial S_2}{\partial t} = d_2 \nabla^2 S_2, \tag{4}$$

with boundary condition

$$C_2 \to C^*, \quad S_2 \to S^*, \quad \text{as} \quad r \to \infty, \tag{5}$$

accompanying with the interface boundary condition for the both layers

$$D_1 \frac{\partial C_1}{\partial r} = D_2 \frac{\partial C_2}{\partial r}, \quad d_1 \frac{\partial S_1}{\partial r} = d_2 \frac{\partial S_2}{\partial r}, \quad \text{at} \quad r = R + a. \tag{6}$$
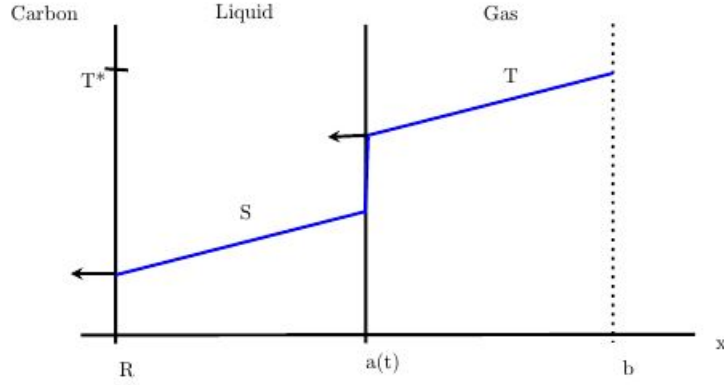
6

Figure 4: Simplified schematic of activated carbon surrounded by sulfuric acid ($H_2SO_4$) and sulfur dioxide ($SO_2$).

Considering the fact that the the spacing between catalyst is small in comparison to catalyst radius the geometry described in Figure 3, the problem reduces to unidirectional model as illustrated in Figure 4, and also assuming the diffusion equation for $O_2$ and $SO_2$ in both gas and liquid layers are quasi static, the equations (2) and (4) simplify to

$$S_{XX} = 0, \quad T_{XX} = 0, \tag{7}$$

where $S$ and $T$ are concentration of $SO_2$ in the liquid and gas layers; respectively, subjected to the boundary conditions

$$d_2 S_X = \alpha \lambda S^\alpha \quad \text{at} \quad X = 0, \quad \kappa S = T, \quad d_2 S_X = d_1 T_X \quad \text{at} \quad X = a(t), \quad T = T^* \quad \text{at} \quad X = b. \tag{8}$$

The first equation in (8) simply describes how much $SO_2$ reacts with the catalyst, here $\lambda$ relates to the rate of reaction and $\alpha$ is related to schewmetric coefficient, which is 1 or 2 (for simplicity we consider $\alpha = 1$). $\kappa$ is just a coefficient for the interface $SO_2$ concentration and $T^*$ is initial sulfur dioxide concentration.

In order to close the model, we need an equation to describe evolution of $a$. Note that all of the produced liquid at the catalyst surface makes the boundary of liquid and gas moves, therefore $a$ evolves as

$$\dot{a} = \delta \alpha \lambda S^\alpha, \tag{9}$$

where $\delta$ relates to rate of reaction between sulfur dioxide and catalyst. Solving (7), (8) and (9) together, considering number of catalysts in a filter and porosity of filter $\phi$, give

7

Table 1: Filter parameters

| Parameter | Definition |
|---|---|
| $R = 10^{-5}$ | Catalysts radius |
| $d_1 = 2*10^{-5}$ | Diffusion coefficient of $SO_2$ in gas layer |
| $d_2 = 2*10^{-9}$ | Diffusion coefficient of $SO_2$ in liquid layer |
| $\phi = 0.3$ | Void fraction of filter |
| $\kappa = 10^{-2}$ | Coefficient for the interface $SO_2$ concentration |
| $2H = 10^{-1}$ | Filter thichness |
| $2h = 10^{-3}$ | Channel width |
| $L = 1$ | Filter length |
| $W_{in} = 10^{-3}$ | Total amount of inlet $SO_2$ concentration |
| $\delta = 2*10^{-2}$ | Rate of reaction between sulfur dioxide and catalyst |
| $\lambda = 2.4*10^{-10}$ | Rate of reaction |
| $u = 5$ | Gas velocity in channel |
| $t_{ref} = 2*10^9$ | Long run time |

$$d_1 T_{XX} = \frac{3}{R\phi} F(a,t), \quad \dot{a} = \delta F(a,t), \quad 0 < X < H, \quad 0 < Y < l, \tag{10}$$

where

$$F(a,t) = \frac{t}{\kappa(a/d_2 + 1) + (b-a)/d_1}, \quad b = R\left((1-\phi)^{-1/3} - 1\right), \tag{11}$$

with boundary conditions

$$T_X|_{X=H} = 0, \quad T|_{x=0} = W_{in}, \quad a|_{t=0} = 0, \tag{12}$$

where $W_{in}$ is the filter inlet averaged concentration of $SO_2$ in the channel.

### 2.1.2 Large Scale–Analyze the transport of sulfur dioxide in the gas channel and filter

In this part we match the macroscopic and microscopic models together. The complete advection-diffusion equation for sulfur dioxide concentration in the channel gives

$$\hat{W}_t + u\hat{W}_Z = d_1(\hat{W}_{XX} + \hat{W}_{ZZ}), \tag{13}$$

where $\hat{W}$ is the local concentration of sulfur dioxide in the channel with velocity $u$. With a carefull analysis and averaging along channel gap ($X$ direction) and ignoring diffusion of sulfur dioxide in $Z$ direction, we find out the averaged $SO_2$ concentration $W$ as
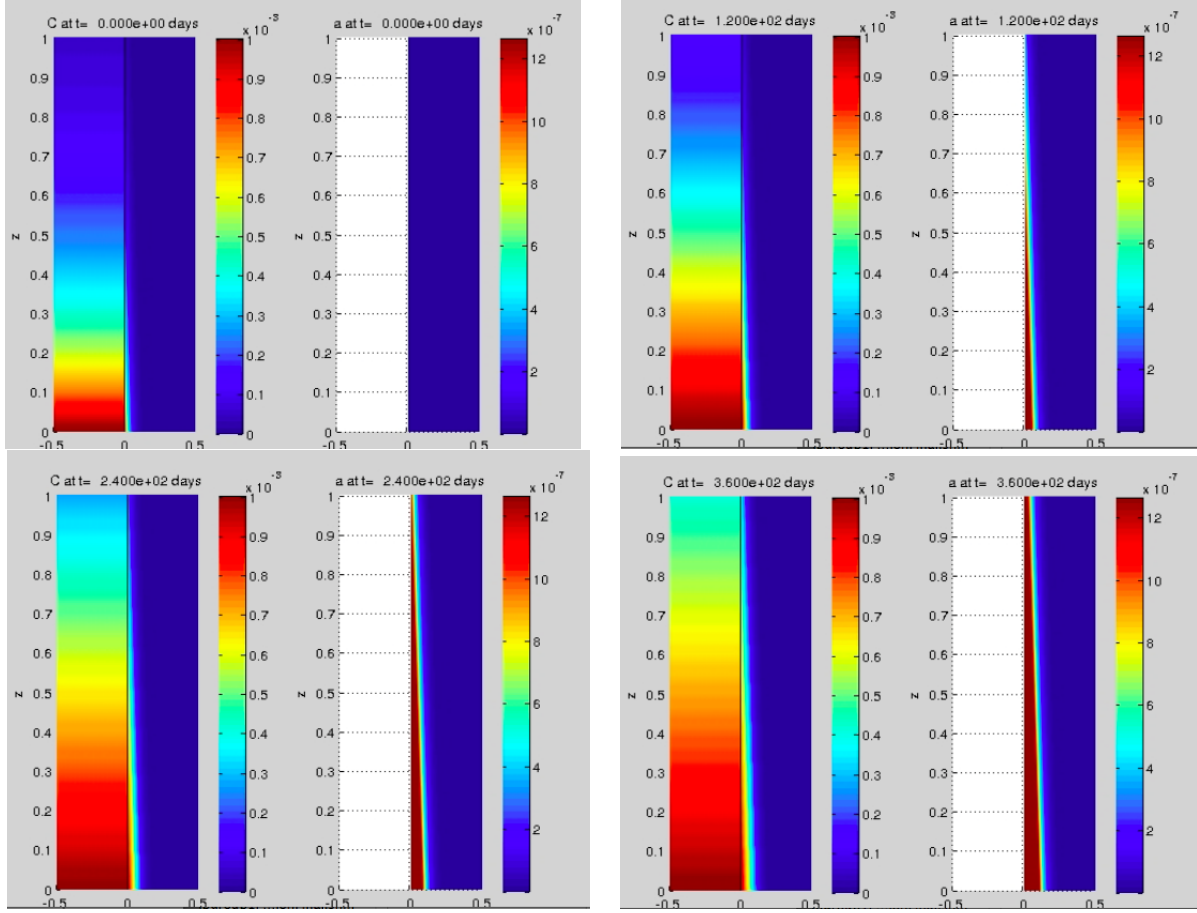
Figure 5: Simulations for sulfur dioxide concentration and evolution of $a$ at (a) initial time, (b) 1200 days, (c) 2400 days and (d) 3600 days. The gas enters from the bottom.

$$\frac{h}{2}uW_Z = d_1\,T_X|_{X=0}\,, \quad \text{for} \quad 0 < Z < L, \quad W(0,t) = W_{in}, \tag{14}$$

where $L = 1\ m$ is the filter length and $W_{in}$ in the total amount of inlet $SO_2$ concentration.

### 2.1.3   Results

Our model has several parameters, which are summarized in the table with their value used in our simulation. Figure 5 shows sulfur dioxide $SO_2$ concentration and evolution of $a$ at several different times. Our results here show that as time passes the liquid is being formed in the filter and most of the formed liquid is at the gas entrance. A common experimental characterization of membrane filtration performance here could be Figure 6, which shows the percentage of filtrate gas versus time. The efficiency here is defined as $1 - W_{out}/W_{in}$. As shown here, filter performance thus ultimately deteriorates, since the formed liquid does not let any interaction happens between the gas and catalysts.
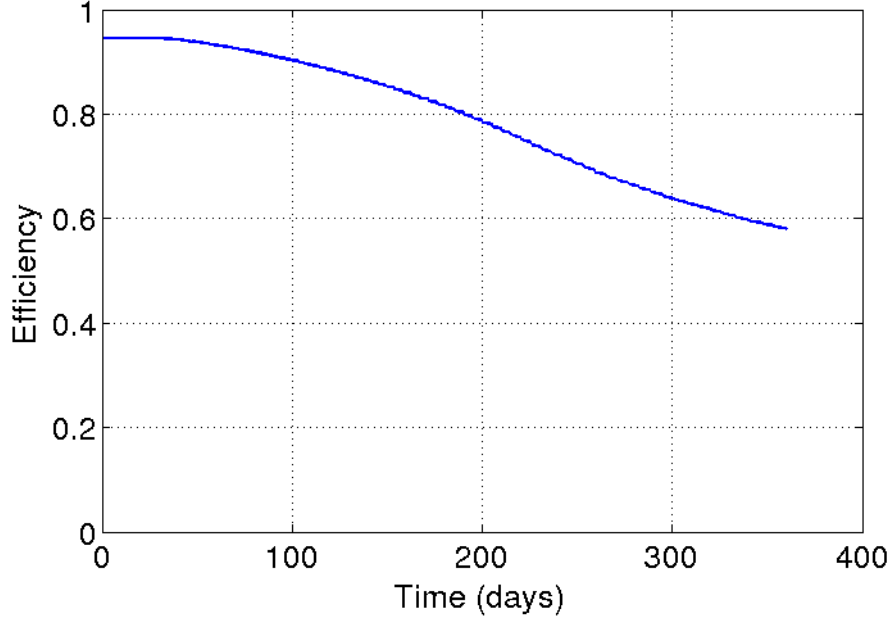
9

Figure 6: Effiviency of a filter versus time.

# 3 Characterization of porous media

## 3.1 Fluid model for membrane filtration

In this sub-problem, our goal was to consider a filter consisting of randomly oriented fibers whose function is to filter out solute from a fluid flowing through it (see Figure 7, similar to the setup in [2,3]). The motivation for answering this question lies in the fact that transport and filtration experiments are easy to carry out in the membrane before it is rolled and compressed into cannisters or cartridges. After the necessary compression step in filter manufacturing, filtration parameters are no longer known. Therefore, we set out to develop the mathematical theory and simulations that would allow prediction of transport properties of the packaged filter.

Our approach is to mathematically characterize an idealized fibrous structure, and use fiber matrix structure theory to relate transport parameters to fiber matrix properties [1–5]. Some of the parameters we model include Darcy permeability of the fluid, void fraction (i.e., void space distribution in the filter), species fraction, effective tracer diffusivity, and the retardation/sieving coefficient. A complete list of the parameters we consider is summarized in Table 2. Ultimately, we are interested in examining how changes in filter compression affect these transport and filtration parameters, as well as the tracer concentration time evolution.

We consider the filtration flow problem through a fiber matrix porous medium, coupled to an advection-diffusion equation for the absorption of tracer to the filter fibers (similar to the
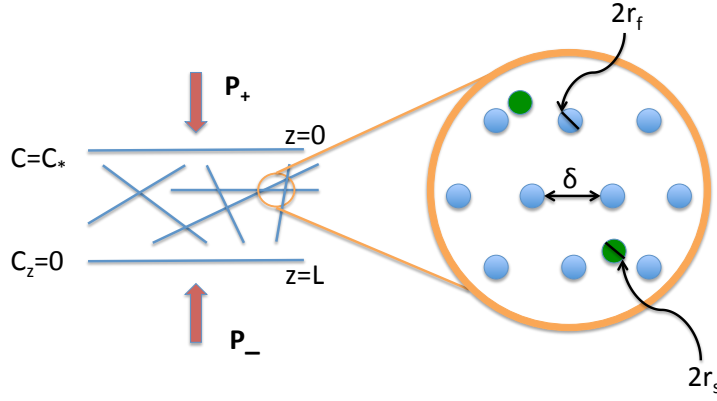
Figure 7: Cartoon of a filter membrane made up of randomly oriented fibers. Fluid flow is modeled through an imposed vertical pressure $p_+$, while the filter bottom is exposed to atmospheric pressure. The right figure zooms in on the fiber matrix structure assumed for the membrane, with some of the parameters indicated in the figure.

approach in [2,3]). We therefore consider Darcy's law relating the fluid velocity to pressure:

$$\boldsymbol{u} = \frac{-K_{p_{eff}}}{\mu}\nabla p \,, \tag{15}$$

where $\boldsymbol{u}$ is the fluid velocity, and $p$ is the fluid pressure.

The continuity equation

$$\nabla \cdot \boldsymbol{u} = 0 \tag{16}$$

then yields

$$\nabla \cdot \left( \frac{-K_{p_{eff}}}{\mu}\nabla p \right) = 0 \,. \tag{17}$$

The advection-diffusion equation for the concentration of tracer is given by:

$$\frac{\partial c}{\partial t} + \frac{1}{\gamma}\nabla \cdot (fc\boldsymbol{u}) = D_{eff}\nabla^2 c \,, \tag{18}$$

where $c$ is the concentration of solute inside filter.

We thus consider the system composed of equations (17) - (18) for our model of fluid filtration

11

Table 2: Fiber matrix structure parameters

| Parameter | Definition |
|-----------|------------|
| $K_{p_{eff}}$ | Darcy coefficient/permeability |
| $\mu$ | fluid viscosity |
| $f$ | retardation/sieving coefficient |
| $\gamma$ | partition coefficient/species volume fraction |
| $\epsilon$ | void fraction |
| $r_f$ | fiber radius |
| $r_s$ | solute particle radius |
| $\delta$ | distance between fiber bundles |
| $A$ | surface area of the tracer |
| $L_u$ | uncompressed membrane thickness |
| $L_c$ | compressed membrane thickness |

through a porous medium membrane. We note that all the parameters in this equation (with the exception of viscosity $\mu$) are dependent on the value of $\epsilon$ (void fraction) of the material considered [1–4]. The expressions for the model parameters are given by:

$$D_{\text{free}} = \frac{kT}{6\pi\mu r_s} , \tag{19}$$

$$D_{\text{eff}} = D_{\text{free}} e^{-\sqrt{1-\epsilon}\left(1+\frac{r_s}{r_f}\right)} , \tag{20}$$

$$\psi = e^{-\sqrt{1-\epsilon}\left(\frac{2r_s}{r_f}+\frac{r_s^2}{r_f^2}\right)} , \tag{21}$$

$$f = 1 - (1 - \psi)^2 , \tag{22}$$

$$K_p = \frac{r_f^2\epsilon^2}{4G(1-\epsilon^2)} , \tag{23}$$

$$G = \frac{2}{3}\frac{2\epsilon^3}{(1-\epsilon)\left(\ln\left(\frac{1}{(1-\epsilon)}\right) - \frac{1}{(1+(1-\epsilon)^2)}\right)} + \frac{1}{3}\frac{2\epsilon^3}{(1-\epsilon)\left(2\ln\left(\frac{1}{(1-\epsilon)}\right) - 3 + 4(1-\epsilon) - (1-\epsilon)^2\right)} , \tag{24}$$

$$\epsilon = 1 - \frac{3r_f^2}{\delta^2} , . \tag{25}$$

We also note that the coupling of the equations occurs through the velocity term $\boldsymbol{u}$ in equation (18).

In terms of boundary conditions, we consider the following for pressure:

$$p(z = 0) = p_+ \tag{26}$$

$$p(z = L) = p_- , \tag{27}$$

where $p_+$ corresponds to the applied pressure of the fluid, and $p_-$ corresponds to the atmospheric pressure (see Figure 7). For the concentration of solute, we impose the following boundary conditions:

$$c(z = 0) = c_+ \tag{28}$$

$$c_z(z = L) = 0 \,, \tag{29}$$

so that the concentration starts at level $c_+$ at the inlet boundary, and there is no flux of solute downstream of the filter.

## 3.2 Uncompressed case for uniform void fraction $\epsilon$

We begin by considering uniform void fraction $\epsilon$, so that it does not depend on concentration. This means that equation (17) for pressure is uncoupled from the system. We also consider the problem in 1D, which reduces the system to:

$$p_{zz} = 0 \,,$$

$$c_t + \frac{f}{\gamma} c_z u = D_{eff} c_{zz} \,.$$

Non-dimensionalization further yields:

$$p_{zz} = 0 \,,$$

$$c_t + \tilde{b} c_z p_z = Pe^{-1} c_{zz} \,, \tag{30}$$

with $\tilde{b} = \frac{fK_p}{\gamma\mu}$, and $Pe$ is the Peclet number: $Pe = \frac{K_p P}{\mu D_{free}}$, where $P = 10$ psi $\approx 68948 \ Pa$ is the pressure scale considered.

The system (30) with boundary conditions (26), (28) is discretized spatially and a Crank-Nicholson time integration scheme is implemented. To account for the nonlinearity in the concentration equation, we set up the system as a Newton's iteration scheme whose solution constitutes the variables at the next time point. Simulations of the system with relevant parameters for the Gore filter membranes are illustrated in Figure 8. We take the concentration initial condition as a piecewise function in the left panel of Figure 8, and assume that the pressure decreases linearly in space from $p_+$ to $p_-$. The right panel of Figure 8 shows the evolution of the concentration profile as time increases. We note that the concentration increases down the membrane, since the model (30) does not account for clogging at the top of the membrane. We also note that the pressure does not change with time, since the pressure simply satisfies the second order equation $p_{zz} = 0$.
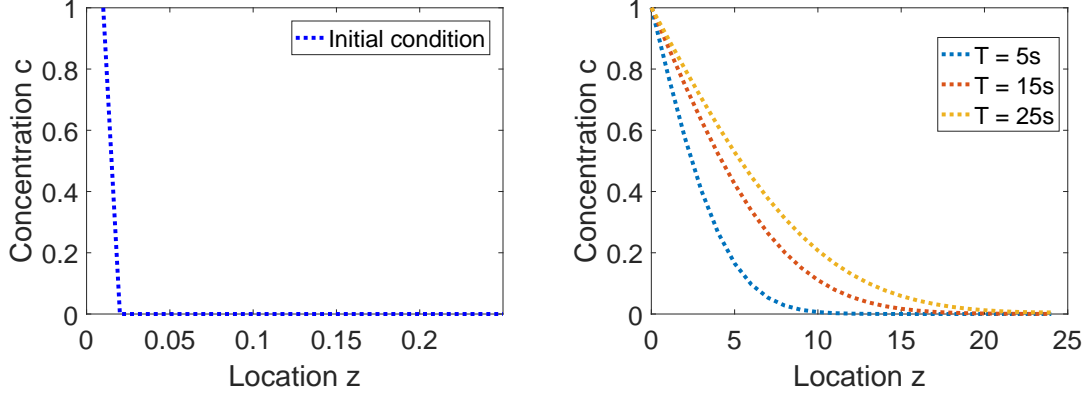
Figure 8: Left: initial condition for the concentration in the uncompressed membrane case. Right: evolution of the concentration profile for $T = 5$s, $T = 15$s, and $T = 25$s.

### 3.2.1 Compressed case for uniform void fraction $\epsilon$

We assume a linear model for the effect of membrane compression on the void fraction $\epsilon$. Assuming that $L_u$ is the uncompressed membrane length and $L_c$ is the length after compression, we have the following equality by conservation of solid mass:

$$AL_u(1 - \epsilon_u) = AL_c(1 - \epsilon_c), \tag{31}$$

where the left side corresponds to the volume of solid in the uncompressed case, and the right side corresponds to the solid volume in the compressed case. Given $\epsilon_u$ from pre-compression experiments, we can therefore choose $\epsilon_c$ satisfying:

$$\frac{1 - \epsilon_u}{1 - \epsilon_c} = \frac{L_c}{L_u}.$$

The results given various compression ratios $\frac{L_c}{L_u}$ are summarized in Figure 9. The differences between the uncompressed and compressed scenarios on the concentration profiles are more pronounced for smaller compression ratios, i.e., more compression of the filter membrane (right column). As mentioned in the previous section, the increase of the concentration down the membrane is due to the absence of clogging in the model.

### 3.3 Mechanical model

Based on the the microstructure of the membrane made of PTFE(possibly), as shown in figure 10, it is possible that the mechanical property of the membrane is highly depend on the fiber length between nodes, based on the microstructure of the membrane, there are several choices of assumptions we can make in order to simplify the problem:
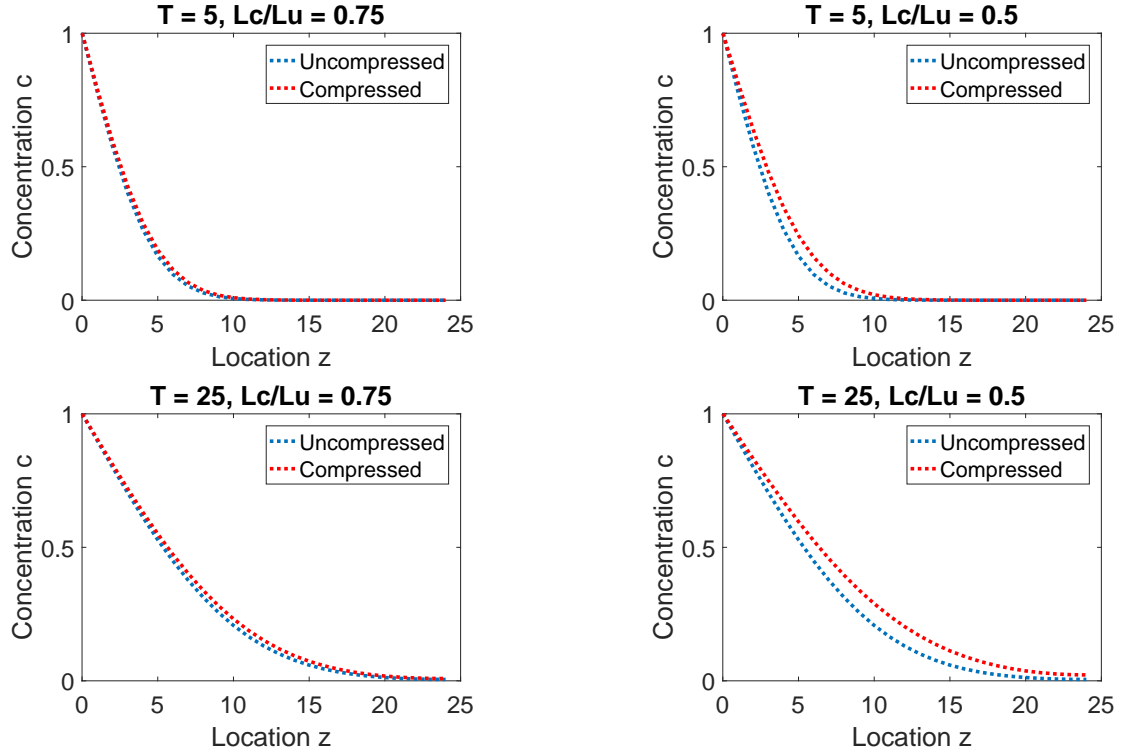
14

Figure 9: Fluid concentration profiles $c$ at times $T = 5$s (top row) and $T = 25$s (bottom row). Compression ratio $L_c/L_u = 0.75$ is shown in the left column, and $L_c/L_u = 0.5$ in the right column.

- fibers (between each nodes) do not bend or buckle but the angles between fibers attached on the same node could change.

- fiber bend and buckle but angles remain the same.
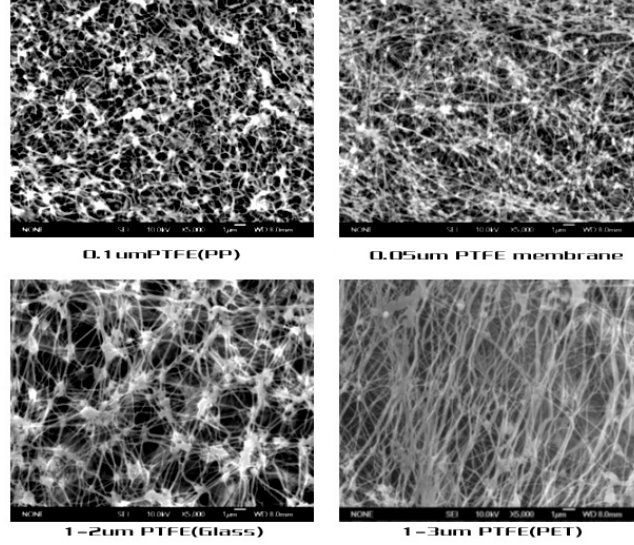
- fiber bend, buckle and the angles could change.



Figure 10: Different microstructures of the membrane of PTFE based on the length of the fiber. see http://www.baghouse.com/products/baghouse-filters/ptfe-filters/

Among the three choices of assumptions, we first discuss the first case which the fibers do not bend or buckle but can be compressed and stretched. We used a method called the stiffness method.

### 3.3.1 Stiffness Method

In the stiffness method, we are going to construct the "stiffness matrix" of the fibrous structure such that

$$f = [K]d \tag{32}$$

where $f$ is the vector represents the forces acting on each node in three directions $(x, y, z)$, $d$ is the vector of the changes of location of each node in three directions $(x, y, z)$. We begin to construct $[K]$ by following steps:

1. Divide the structure into two sets: MEMBERS(fibers or edges) and NODES(knots)

2. For each member, we consider the local relation of the axial forces $(q_1, q_2)$ and displacements $(u_1, u_2)$, and the relation can be written as

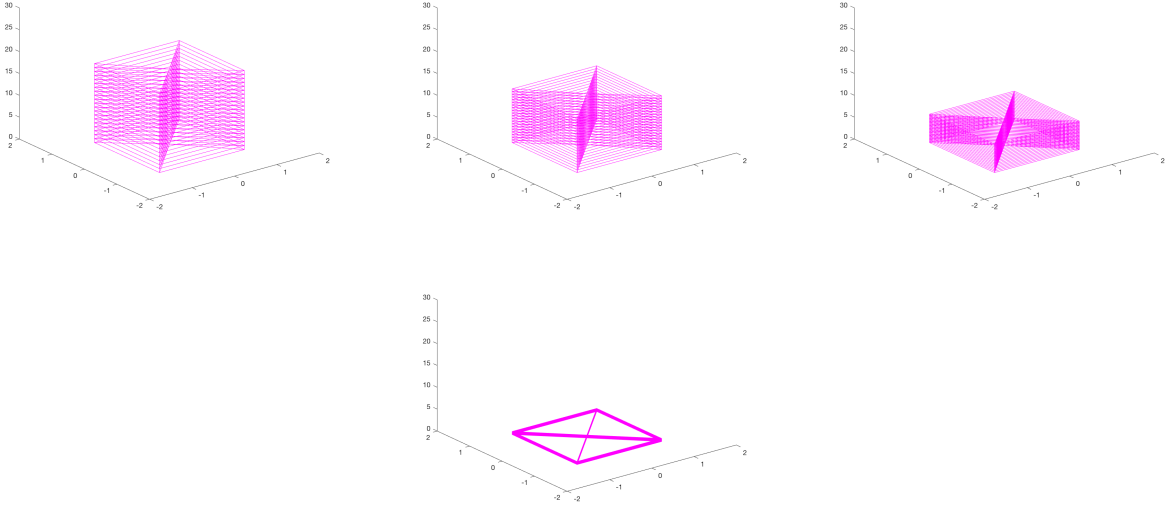$$\mathbf{q} = k\mathbf{u} \tag{33}$$

16

Figure 11: Simulation of compression of a stack of fibrous cube with symmetric connection, this validates our model

where $k = \begin{bmatrix} 1 & -1 \\ -1 & 1 \end{bmatrix}$.

3. Use coordinate transformation to assign the contribution of each member's local displacement and force into the global coordinate system. For each member,

$$\mathbf{u} = T\mathbf{v} \tag{34}$$

$$\mathbf{f} = T^{\mathrm{t}}\mathbf{q} \tag{35}$$

where $T$ is the coordinate transformation matrix, and $T^{\mathrm{t}}$ is the transpose of $T$.

4. Assemble each forces and displacements of each element into one vector $\mathbf{f}$ and $\mathbf{v}$.

For more detailed tutorial, see `http://people.duke.edu/~hpgavin/cee421/truss-3d.pdf`, or
`https://engineering.purdue.edu/~aprakas/CE474/CE474-Ch5-StiffnessMethod.pdf`.
In the simulation, we used the Matlab code "Truss Analysis" written by Hossein Rahami and updated by Frank McHugh. We present the following simulations by compressing a cubic fibrous "rod" and a fibrous cube.
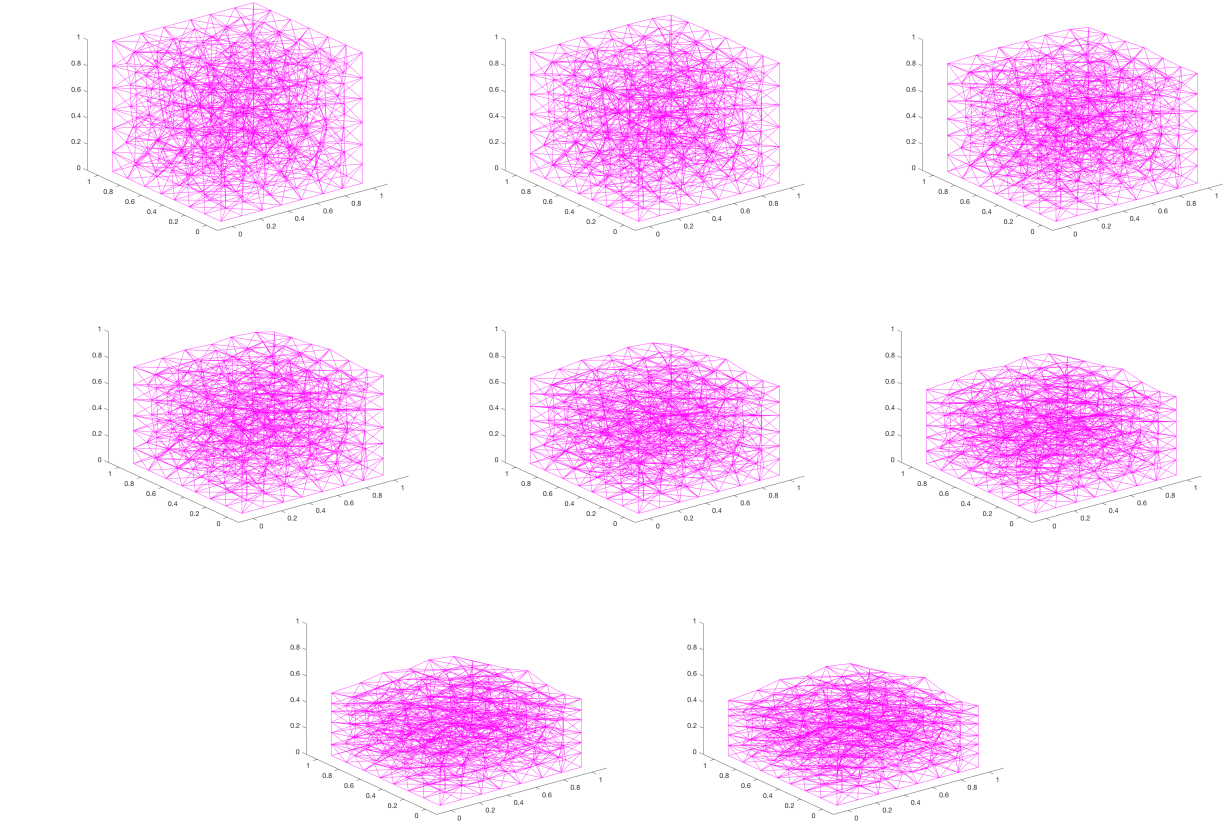
17

Figure 12: Simulation of compression of a fibrous cube whose fibers are extracted from the edges of a meshed cube

### 3.3.2 Remarks

- Random fiber orientations (or random distribution of the nodes) needs to be considered in this model rather than extracting edges from a mesh.

- Boundary conditions needs to be carefully determined, for example, in both compression cases, the nodes on the edges and four sides of the cubes only bear vertical forces, which means we are attaching wheels on all those nodes agains a fixed wall.

## 3.4 Kirchhoff rod theory

Next we pursue a separate approach to contemplate the compression of porous membranes into filters. This is inspired by noting that a porous membrane can be made of a fibrous mesh that traps particles between the fibers. We will model the effects of compression on the shape of a single fiber, by considering a fiber to be a planar Kirchhoff rod. This places us in the context of the theory of finite displacement (via bending and twisting) of thin rods. Deformations of infinitesimal pieces of the rod may be small, but can effect a large deformation of the rod as a whole.

### 3.4.1 Derivation of ODE System

Consider the centerline of a rod to be a curve in the xz-plane, with position parameterized by arc length $s$ as follows

$$\overrightarrow{r}(s) = x(s)\hat{i} + z(s)\hat{k}. \tag{36}$$

Take $\hat{e}_1(s)$ to be the unit normal vector to the curve and $\hat{e}_3(s)$ to be the unit tangential vector to the curve, so that

$$\hat{e}_3 = \frac{d\overrightarrow{r}}{ds} = x'(s)\hat{i} + z'(s)\hat{k}. \tag{37}$$

We must also take into account the rod curvature $\kappa$, which corresponds to the direction $\hat{j}$ out of the page via the unit binormal vector $\hat{e}_2(s)$. Let

$$\overrightarrow{k} = \kappa\hat{j} = \kappa\hat{e}_2.$$

By definition, curvature of a smooth curve with position vector $\overrightarrow{r}(s)$ and unit tangent vector $\hat{e}_3(s)$ is given by

$$\kappa = \left\| \frac{d\hat{e}_3}{ds} \right\|.$$

Accordingly, we have

$$\frac{d\hat{e}_3}{ds} = \overrightarrow{k} \times \hat{e}_3, \tag{38}$$

and similarly,

$$\frac{d\hat{e}_1}{ds} = \overrightarrow{k} \times \hat{e}_1 \,. \tag{39}$$

Then substituting for $\overrightarrow{k}$ and $\hat{e}_3$ in equation (38) implies

$$\begin{aligned}
\frac{d\hat{e}_3}{ds} &= \kappa\hat{j} \times [x'(s)\hat{i} + z'(s)]\hat{k} \\
&= \kappa[z'(s)\hat{i} - x'(s)\hat{k}] \,.
\end{aligned} \tag{40}$$

Now define $\phi(s)$ to be the tangent vector's angle from the x-axis, with $x'(s) = \cos(\phi)$ and $z'(s) = \sin(\phi)$, so that by substitution into equation (40),

$$\frac{d\hat{e}_3}{ds} = \kappa[\sin(\phi)\hat{i} - \cos(\phi)\hat{k}] \,; \tag{41}$$

and also by substitution into equation (37),

$$\hat{e}_3 = \cos(\phi)\hat{i} + \sin(\phi)\hat{k} \,, \tag{42}$$

which implies

$$\frac{d\hat{e}_3}{ds} = -\sin(\phi)\frac{d\phi}{ds}\hat{i} + \cos(\phi)\frac{d\phi}{ds}\hat{k} \,. \tag{43}$$

Equating the right hand sides of equations (41) and (43), we derive for curvature

$$\kappa = -\frac{d\phi}{ds} \tag{44}$$

Furthermore, from equations (38) and (41) we have that

$$\hat{e}_1 = \hat{e}_2 \times \hat{e}_3 = \sin(\phi)\hat{i} - \cos(\phi)\hat{k} \tag{45}$$

Keeping in mind this planar representation of a curve (the centerline of our rod), we use constitutive relationships between moments and curvature to derive an eighth-order ODE system describing the curve's deformation due to a load at its ends. This will represent a single fiber in a fibrous membrane under compression.

Let $\overrightarrow{F}(s)$ be the force vector and $\overrightarrow{M}(s)$ be the moment vector. Recall that the moment measures the tendency of the force to rotate the object (such as our rod) about a point or axis. Let $E$ be Young's modulus and $I$ be the moment of inertia of a cylinder, and recall curvature $\kappa$. Then for the force and the moment, respectively, we have:

$$\overrightarrow{F} = F_1(s)\hat{e}_1 + F_3(s)\hat{e}_3 \,, \tag{46}$$

20

and

$$\overrightarrow{M} = EI(\kappa - \kappa''(s))\hat{e}_2 \,. \tag{47}$$

Taking the derivative of both sides of equation (47) with respect to $s$, recalling $\frac{d\hat{e}_2}{ds} = 0$, we get

$$\overrightarrow{M}'(s) = EI\frac{d}{ds}[\kappa - \kappa'']\hat{e}_2 \,,$$

which implies

$$\frac{M_2}{EI} = \kappa - \kappa'' \,. \tag{48}$$

From the balance of linear and angular momentum, according to general Kirchhoff rod theory, we have relationships

$$\overrightarrow{F}''(s) = \overrightarrow{0} \tag{49}$$

and

$$\overrightarrow{M}'(s) + \hat{e}_3 \times \overrightarrow{F} = \overrightarrow{0} \,. \tag{50}$$

Substituting equation (46) into equation (50) implies

$$M_2' = -F_1 \,. \tag{51}$$

Next, taking the second derivative of equation (46) and substituting equations (38) and (39), we see that the constitutive force equation (49) implies

$$\overrightarrow{F}'' = [F_1'' - \kappa^2 F_1 + \kappa' F_3 + 2\kappa F_3]\hat{e}_1 + [F_3'' - \kappa^2 F_3 - \kappa' F_1 - 2\kappa F_1']\hat{e}_3 = 0 \tag{52}$$

### 3.4.2 Kirchhoff Rod ODE System

Thus, from equations (44), (48), (51), and (52), we extract the eighth-order ODE system describing the rod's centerline:

$$
\begin{aligned}
\phi'(s) &= -\kappa \\
\kappa'' - \kappa &= \frac{-M_2}{EI} \\
M_2' &= -F_1 \\
F_1'' &= \kappa^2 F_1 - \kappa' F_3 - 2\kappa F_3' \\
F_3'' &= \kappa^2 F_3 + \kappa' F_1 + 2\kappa F_1'
\end{aligned}
\tag{53}
$$

We can solve this system in MATLAB, given eight boundary conditions. The conditions we

consider to start with include no shear force at the rod ends

$$F_1(0) = F_1(L) = 0 \,, \tag{54}$$

a load at the ends (the compression force)

$$F_3(0) = -F_3(L) = -N \,, \tag{55}$$

constant curvature at the rod ends

$$\kappa'(0) = \kappa'(L) = 0 \,, \tag{56}$$

no torque at the bottom, such as from fixing the rod to the base

$$M_2(0) = 0 \,, \tag{57}$$

and the rod standing straight up at the base

$$\phi(0) = \pi/2 \,. \tag{58}$$

## 3.5 Future work

**Fluid flow through filters**

In the fiber matrix model described in Section 3.1, we considered fluid flow through a filter membrane, and prescribed boundary conditions for the pressure on the top and bottom of the membrane. A more realistic boundary condition that we plan to implement is prescribing the flow $Q = -\frac{K_p}{\mu} A p_z$ at the inlet boundaries rather than the pressure, as this may be more easily available from experiments. Moreover, a more realistic model for the fluid flow can be explored by introducing clogging through the equation:

$$\frac{d\xi}{dt} = kc \,, \tag{59}$$

where $\xi$ corresponds to the amount of bound solute, and $k$ is a rate parameter. This $\xi$ is subsequently subtracted from equation (25) for void fraction $\epsilon$, making all other parameters also dependent on $\xi$ (and therefore time-varying). This will yield a dynamic pressure distribution, and will fully couple equations (17) - (18).

**Mechanical fiber model**

For the mechanical model presented in Section 3.3, we propose the following improvements:

- Random distributed fibers needs to be applied.

- Buckling of the fibers needs to be considered by adding two more components $\phi$, $\theta$ on the unknown vector $\mathbf{u}$ which denotes the angular momentum in 3D.

- Mechanical properties of the membrane should be considered for the realistic case.

- Find a way to get the filter parameters as well as the changes of the macroscopic level from the microscopic level simultion, i.e. bubble point, porosity, etc.

- A more realistic boundary condition needs to be considered. For example, if the nodes on the edges or surfaces of the cube are allowed to move horizontally, some of the nodes might be compressed "out of" the cube and the deformation of those fibers attached to the nodes are very large, which is unrealistic. Therefore buckling or even failure of such fibers shall be considered.

## 4    Acknowledgements

## References

[1] F. CURRY, *Mechanics and thermodynamics of transcapillary exchange*, Handbook of physiology, 4 (1984), pp. 309–374.

[2] Y. HUANG, D. RUMSCHITZKI, S. CHIEN, AND S. WEINBAUM, *A fiber matrix model for the growth of macromolecular leakage spots in the arterial intima*, Journal of biomechanical engineering, 116 (1994), pp. 430–445.

[3] Y. HUANG, D. RUMSCHITZKI, S. CHIEN, AND S. WEINBAUM, *A fiber matrix model for the filtration through fenestral pores in a compressible arterial intima.*, The American journal of physiology, 272 (1997), pp. H2023–39.

[4] J. LEVICK, *Flow through interstitium and other fibrous matrices*, Quarterly journal of experimental physiology, 72 (1987), pp. 409–437.

[5] C. MICHEL, *Fluid movements through capillary walls*, Handbook of Physiology. The Cardiovascular System. Microcirculation, 4 (1984), pp. 375–409.